

Supporting Information

Efficient Delivery of Oxygen via Magnetic Framework Composites

Leena Melag, † M. Munir Sadiq, *‡ Stefan J. D. Smith, ‡ Kristina Konstas ‡, Kiyonori Suzuki, *|| and
Matthew R. Hill, *†‡

†Department of Chemical Engineering, Monash University, Clayton, VIC 3168, Australia

|| Department of Materials Science and Engineering, Monash University, Clayton, VIC 3168,
Australia

‡ CSIRO, Private Bag 33, Clayton South MDC, VIC 3169, Australia

*Email - matthew.hill@csiro.au

1. Experimental

All reagents and solvents used for the synthesis were obtained from commercial vendors and used as received.

I. Synthesis of Co-MOF-74

0.75 g of 2, 5-dihydroxyterephthalic acid (DHTA) and 3.0 g of $\text{Co}(\text{NO}_3)_2 \cdot 6\text{H}_2\text{O}$ were dissolved in 150 mL of DMF. The mixture was sonicated in a 250 mL Duran bottle and placed in an oven at 110°C for 20hrs. On cooling down to room temperature, the mother liquor was decanted and the products were washed with DMF three times and then immersed in methanol. The methanol was exchanged with fresh methanol for the next six days and the samples were activated at 250°C under vacuum for 24 hrs and stored in a N_2 glove bag.^{1,2}

II. Synthesis of Fe_3O_4 Nanoparticles

Hydrophilic Fe_3O_4 nanoparticles were synthesized using a facile one step method. First, trisodium citrate (1 mmol, $\text{C}_6\text{H}_5\text{Na}_3\text{O}_7 \cdot 2\text{H}_2\text{O}$), sodium hydroxide (4 mmol), and sodium nitrate (0.2 mol) were dissolved into deionized water (19 mL) and heated to 100 °C. 1 mL of 2M $\text{FeSO}_4 \cdot 4\text{H}_2\text{O}$ (2mmol) solution was added to the mixture it and the entire solution was maintained at 100 °C for one hour. After cooling, the black precipitate was magnetically separated from the solvent and redispersed into DI water and can be stored in water for up to a month.³

III. Synthesis of the (Co-MOF-74-Fe₃O₄) composite

The synthesis of Fe₃O₄ nanoparticles had citrate and sodium nitrate salts, resulting in citrate capped Fe₃O₄ nanoparticles. Therefore, no separate attempt was made to functionalize the surfaces of these magnetic nanoparticles. As these nanoparticles having a tendency to agglomerate and settle down, the mixture of Co-MOF-74 precursor and preformed Fe₃O₄ nanoparticles was subjected to continuous mechanical stirring for the entire duration of 2 and half days at a temperature of 100°C . For the washing cycles, the composites were magnetically separated from the solvents. For this study, composites with 0.08 wt % (MC1) , 8.8 wt % (MC2) , 11.8 wt % (MC3) , 12.18 wt % (MC4) , 12.6 wt % (MC5) , and 15 wt % (MC6) of magnetic nanoparticles were synthesized.^{1,2}

2. Powder X-ray diffraction

The phase identification studies were conducted using a Phillips PW-1140 with a Co-K α radiation of 1.79 Å at 40 kV and 25 mA. As shown in Fig. S1 a) and b), the XRD pattern of the synthesised Fe₃O₄ nanoparticles (reference pattern for a cubic spinel Fe₃O₄ lattice) and the composites are in agreement with literature reports. As can be observed from the XRD patterns in Fig. S1 b), there is a gradual shift in the peak positions of composites MC5 and MC6, that have higher concentrations of magnetic nanoparticles.

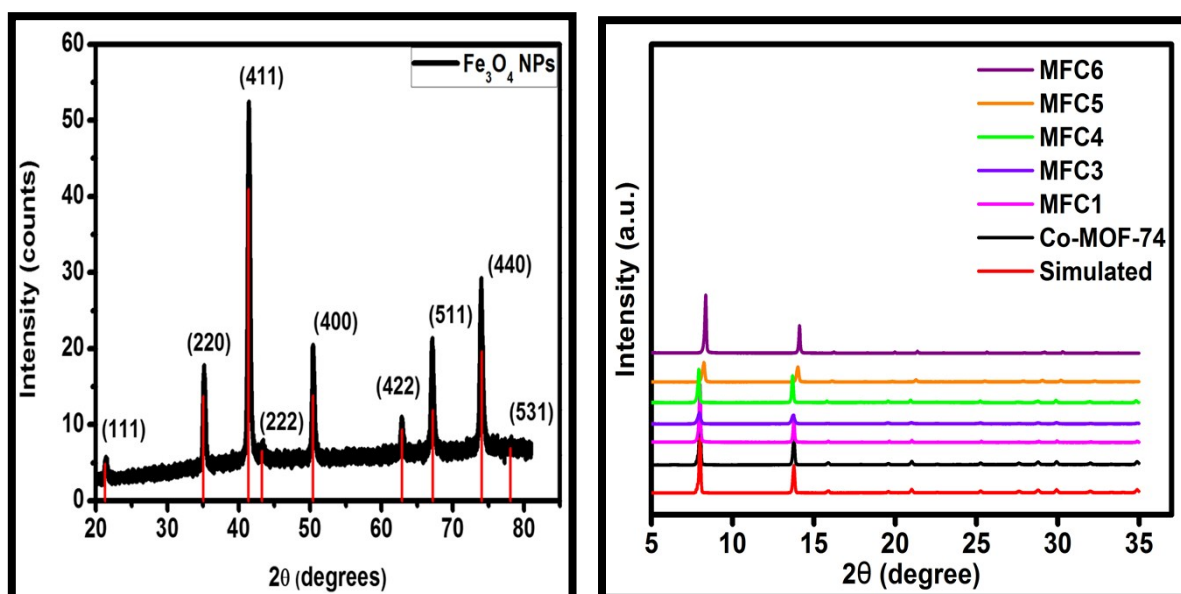


Fig. S1: The powder X-ray diffraction patterns of a) the synthesised Fe₃O₄ nanoparticles that can be referenced to the theoretical patterns for a cubic Fe₃O₄ lattice (COD 1011084), and b) the synthesised Co-MOF-74 and simulated data and the composites with varying concentrations of magnetic nanoparticles.

3. Microstructural Analysis

The morphological studies on the samples were carried out using the JOEL 7001F Scanning Electron Microscope. The micrographs show hexagonal-shaped prism aggregates of Co-MOF-74 crystals with solid elongated structures measuring a few μm in length.

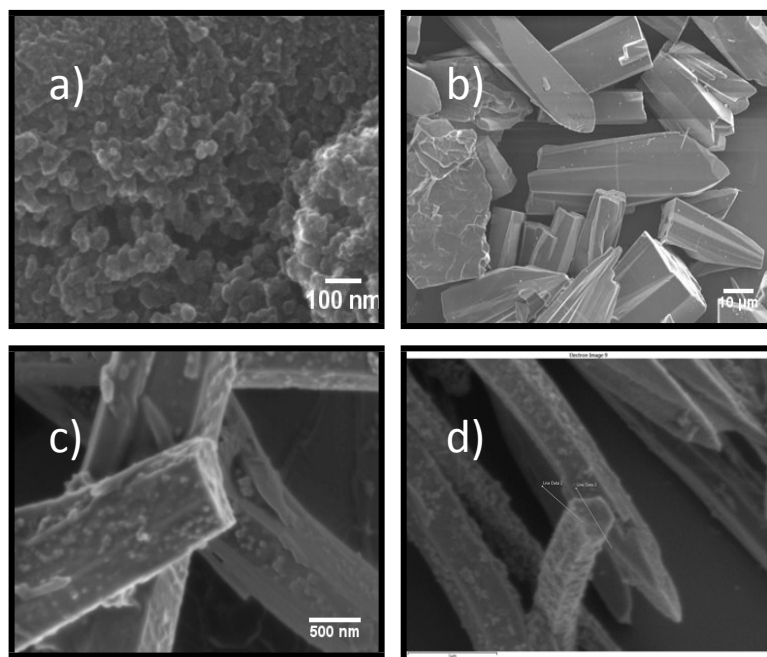


Fig.S2 : SEM Images of a) the synthesized Fe_3O_4 nanoparticles in the size range of 20-100nm. b) hexagonal-shaped prism aggregates of Co-MOF-74 crystals with solid elongated structures measuring a few μm in length, c) and d) the Fe_3O_4 -composite with the magnetic nanoparticles embedded on its surface.

4. Thermogravimetric analysis

For the thermogravimetric analysis, the MOF samples were heated from the room temperature to 600 $^{\circ}\text{C}$ at 20 $^{\circ}\text{C}/\text{min}$ in a nitrogen atmosphere. The thermal treatment on the bare MOF and the composite showed an initial gradual loss in weight for both, but after 300 $^{\circ}\text{C}$, the composite collapsed faster than the bare MOF leading to a more drastic weight loss around 500 $^{\circ}\text{C}$ for the final structural collapse .⁴

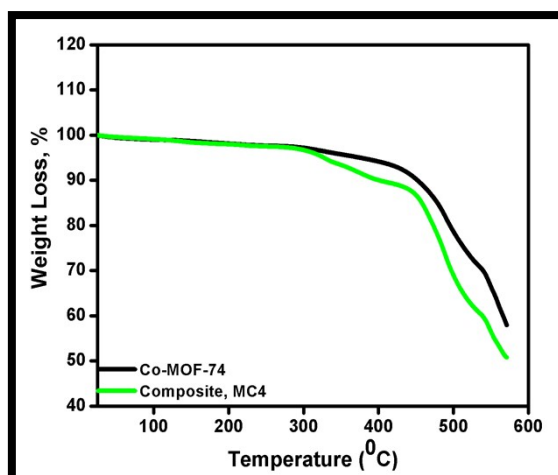


Fig. S3: Comparison of the TGA curves of the bare Co-MOF-74 and the Magnetic framework composite, MC4.

5. Low pressure gas adsorption analysis

To determine the surface area and porosity properties of the bare Co-MOF-74 and the MFCs, 10 - 50 mg of dry sample was transferred into the BET glass tube, it was capped with a transeal and weighed. The tubes were fixed onto a Micrometrics ASAP 2020 gas adsorption analyzer where the samples were heated to 250 °C under dynamic vacuum for 24 hrs and weighed again. Low-pressure N₂ adsorption isotherms were carried out at 77K at preset measurement data points to collect the nitrogen adsorption-desorption data over a broad range of pressures.

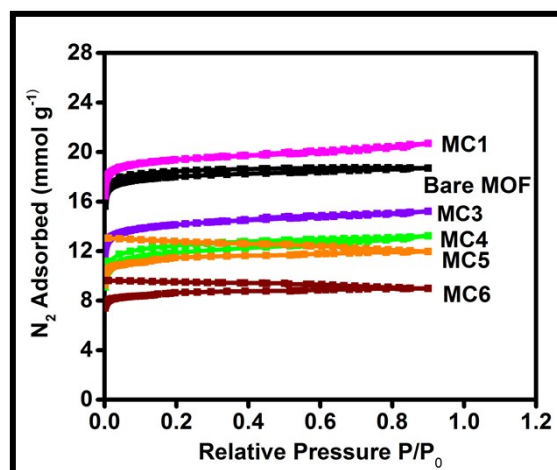


Fig. S4: N₂ Adsorption isotherms of Co-MOF-74 and MFCs at 77K.

	Bare	MC1	MC3	MC4	MC5	MC6
--	------	-----	-----	-----	-----	-----

	MOF	(0.08 wt. %)	(11.8 wt. %)	(12.18 wt. %)	(12.6 wt. %)	(15 wt. %)
BET (m ² /g)	1449	1478	1082	1008	953	713
Langmuir (m ² /g)	1764	1909	1399	1150	1247	933

Table S1: Results from the surface area measurements of the bare Co-MOF-74 and the MFCs.

In real air separation, 400 ppm of CO₂ is present and its capture is facilitated in a pre-purification process by using either absorption, adsorption, cryogenic distillation or membrane separation. To understand the effect of trace quantities of CO₂ we carried out the CO₂ adsorption study at 204 K. As expected, the uptake of CO₂ by MOF-74 at 204 K is much higher than of oxygen, particularly at low partial pressures, indicating that a pre-purification step is required to remove carbon dioxide and water from the process.

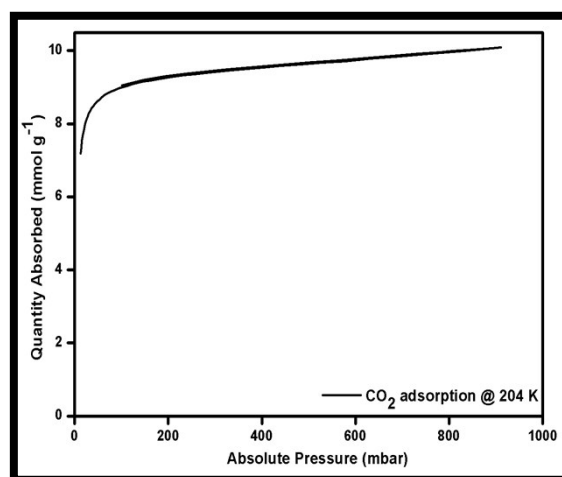


Fig. S5: CO₂ Adsorption isotherms of Co-MOF-74 at 204K.

6. Vibrating Sample Magnetometer

The saturation magnetization (M_s), coercivity (H_c) and magnetization curves were studied on a vibrating sample magnetometer (VSM, RIKEN DENSHI) operated at room temperature. The samples are prepared by embedding the magnetic nanoparticles in an epoxy resin and hardener mix and once it was all set, the measurements were carried out. The results of the synthesized Fe₃O₄ nanoparticles show a saturation magnetisation of 58 emu/g and with MFCs, the saturation magnetization values were higher for composites with higher concentrations of magnetic nanoparticles, MC6 (1.6 emu/g), MC5 (1.2 emu/g), MC4 (1 emu/g), MC3 (0.8 emu/g) and MC2 (0.1 emu/g).

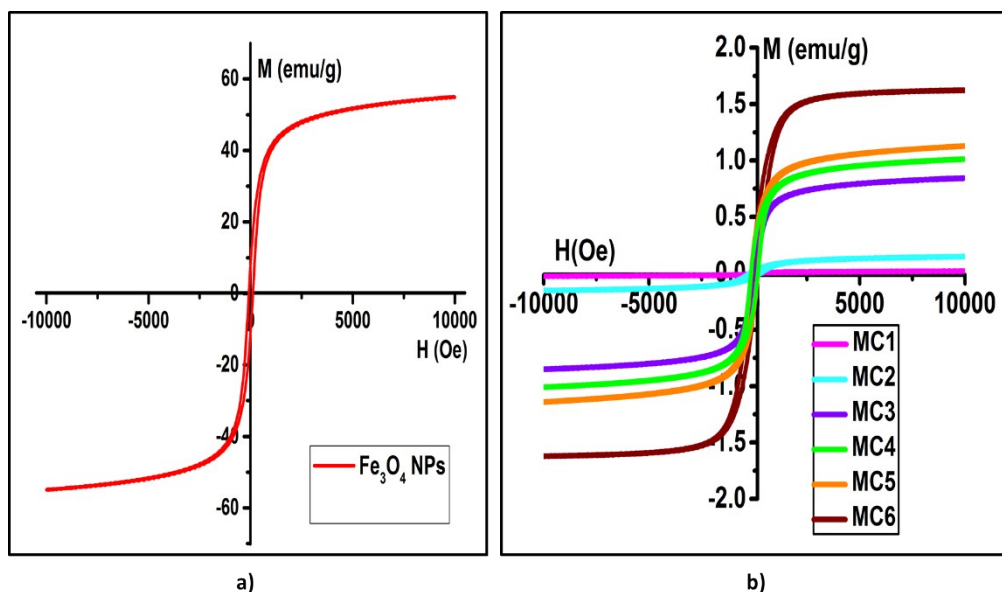


Fig. S6: Hysteresis loop of a) Fe_3O_4 nanoparticles and the b) MFCs.

7. Thermo-magneto gravimetric Analysis

The Curie temperature of the Fe_3O_4 nanoparticles was determined using the Thermo-magneto gravimetric analysis which is a very efficient technique to ascertain the various structural and magnetic transitions in the nanoparticles. Basically Curie point is the temperature at which a sharp change in the magnetic properties is observed, and the otherwise strong magnetic properties of the material are lost and it becomes paramagnetic. This is derived by measuring the change in weight of the sample as a function of temperature, in an applied magnetic field.^{1, 5-7 8} The change in temperatures cause changes in magnetic properties of the samples that is noticed by the change in the weight of the sample. This principle is used to determine the Curie temperature. Here the measurements on a weighed amount of Fe_3O_4 nanoparticles were conducted by heating it from room temperature to 1000 °C in a nitrogen atmosphere using a heating rate of 40 °C/min and the Curie temperature for the synthesized Fe_3O_4 nanoparticles was found to be $T_c=570$ °C. This self-controlling heating property of the magnetic nanoparticles is used in applications as a control to avoid overheating.

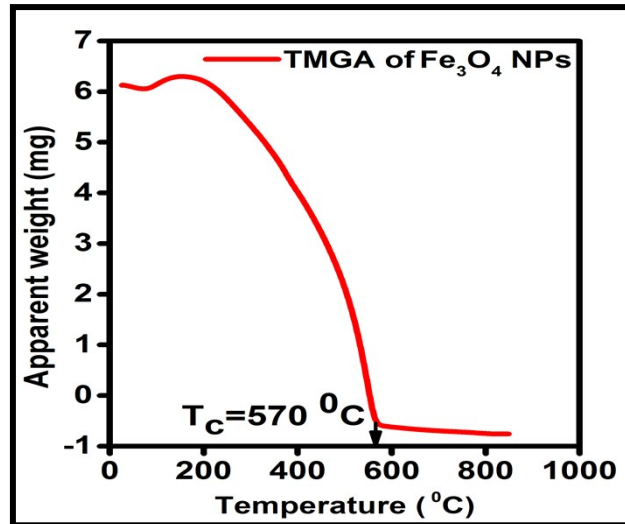


Fig. S7: Using Thermo-magneto-gravimetric analysis, the Curie temperature of the synthesized Fe_3O_4 nanoparticles was found to be $T_c=570\text{ }^\circ\text{C}$.

8. Specific Absorption Rate (SAR).

Specific Absorption Rate, SAR, describes the heating efficiency of the magnetic materials and indicates the rate at which the magnetic nanoparticles will absorb the magnetic energy and convert it into thermal energy. Apart from the diameter, shape and composition of the nanoparticles, SAR is strongly governed by the frequency of the applied magnetic field. In hyperthermia treatments nanoparticles with high SAR values are preferred because it means a higher absorption rate even at low concentrations. ⁷ SAR is calculated by dispersing the particles in a liquid medium and the measuring:

$$\text{SAR} = \frac{C_s m_s}{m_m} \left(\frac{dT}{dt} \right)_{t=0} \quad 8.1$$

Where C_s is the specific heat capacity of suspension, dT/dt at $t=0$ is the initial gradient of the heating curve, m_s and m_m are the specific masses of the suspension and magnetic particles, respectively. The units of SAR are watts per kilogram (W/kg).^{9, 10} To measure SAR, the nanoparticles were dispersed in water at a concentration of 5mg/ml. This magnetic suspension was placed in a dewar flask and exposed to an induction heating system (EASYHEAT 0224–Ambrell) with a heating coil of 8 turns (N) of 2.5 cm diameter (D) and 4 cm in length (L). The amplitude of the AC magnetic field was fixed at $H = 13.09$ kA/m. The temperature rise attained by the samples for the next 30 minutes is noted

as the heat generation capacity of the samples. An IR Thermal camera (FLIR E5) was used to capture these changes in the temperatures. With the initial starting temperature of 23.84 °C, and on exposure to an AC magnetic field, the Fe₃O₄ nanoparticles stabilized at a temperature of 85.02 °C and the MFC exhibited a maximum temperature rise (T_{max}) of 63.7 °C. The SAR values calculated using equation (8.1) are 74.48 W/g for the Fe₃O₄ nanoparticles and 14.19 W/g for the Fe₃O₄-composite.

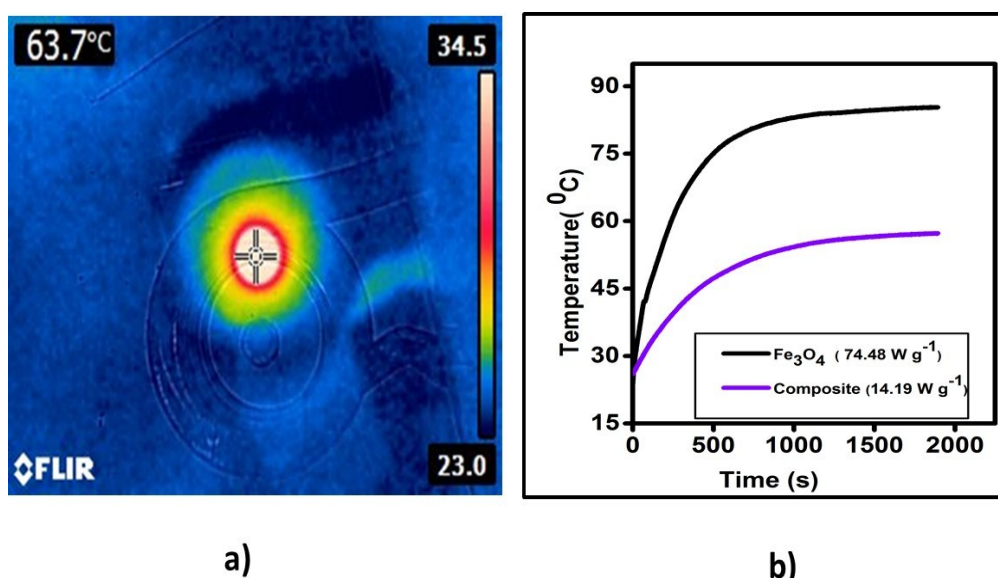


Fig. S8: SAR measurements: a) The live image captured by the IR-camera of the temperature rise attained by the MC3 composite, b) The calculated specific absorption rate values of 74.48 W/g for the Fe₃O₄ nanoparticles and 14.19 W/g for the Fe₃O₄-composite.

9. Set- up for the Magnetic Triggered Release of Oxygen

The triggered release of oxygen from the MFC was achieved using the Tristar Micrometrics adsorption equipment and the EASYHEAT Ambrell induction-heating machine. The set-up consisted of a glass tube with the sample in it, which was hooked on to the Tristar Micrometrics Adsorption machine. A slightly bigger glass tube, acting as a dewar and containing the acetone+dry ice mixture was encircling the sample tube. This setup was fitted through an induction coil in such a manner that the sample comes in the center of the 8-turn coil. This ensured uniform exposure of the sample to the magnetic field. The effects of the magnetic field were contained using a Faradays cage.

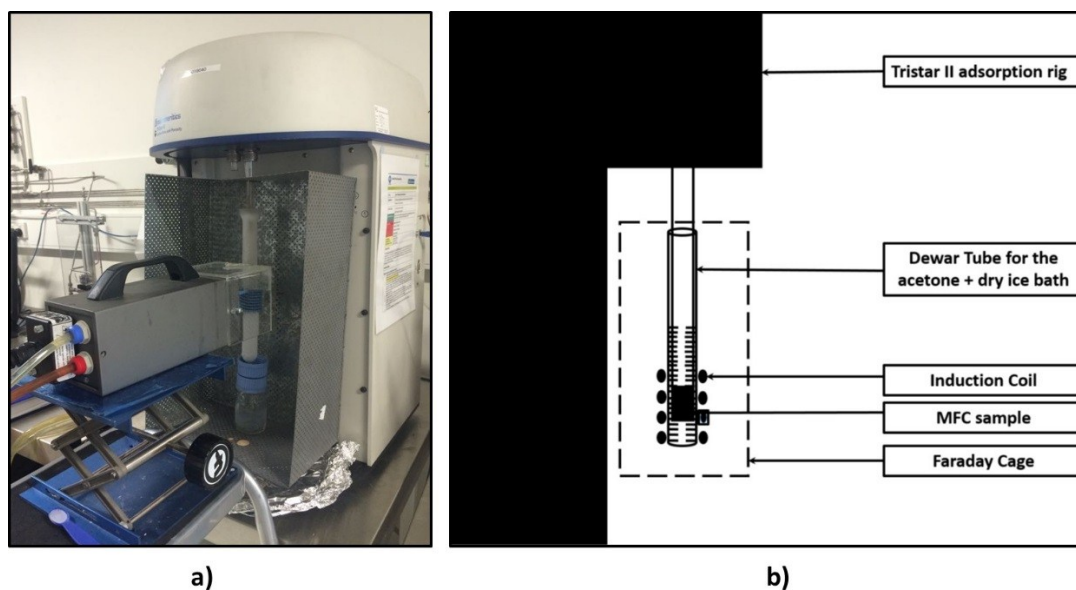


Fig. S9: Set-up for the triggered release of oxygen, a) The actual set-up of the sample tube attached to the Tristar Micrometrics adsorption equipment and the EASYHEAT Ambrell induction-heating machine used to facilitate the heating of the magnetic nanoparticles, b) the graphical representation of the same set-up.

During calculations of SAR, using a magnetic field strength of 16.4 mT, the Fe_3O_4 nanoparticles stabilized at a temperature of 63.7 °C. Therefore to achieve this temperature of 63.7 °C, a current of 78A had to be passed through the 8-turn coil of the EASYHEAT Ambrell induction heating system.

Based on these calculations, the first set of triggered release was carried out by passing 78A current (63.7 °C) through the coils. However, the experiments for calculation of SAR are carried out at room temperature whereas these triggered release experiments are carried out at temperatures of -69 °C. Therefore due to the cold acetone + dry ice bath encircling the sample, the maximum desorption temperatures were not reached and complete desorption of oxygen molecules was not achieved. To target maximum desorption, the temperatures were increased by increasing the current passing through the coil. Finally, the maximum desorption from the composites was achieved when a current of 83.2 A was passed through the coil generating a magnetic field strength of 17.4 mT to overcome the cold barrier of the acetone-dry ice bath and cause localised heating of the Fe_3O_4 nanoparticles, which otherwise, in these settings, would have attained the temperatures of 68.5 °C .

Table S2: Magnetic Field Settings

Current through the coil, A	Magnetic Field Strength, mT	Temperature °C
78	16.5	63.8
79.3	16.7	64.8
81.9	17.2	66.9
83.2	17.4	68.5

10. Regeneration energy calculations:

For a cryogenic distillation based Air Separation Unit producing 110 to 350 tonnes of oxygen per day, the specific energy is reported as 1.11 MJ/kg- 1.82 MJ/kg at 40 bar. (Air Liquide Engineering & Construction. Standard Plants. 04-2017).

At this early lab scale set-up it is not possible to directly determine energy use for the process, but the energy calculations for the estimated regeneration energy (Q_{thermal}) of our composite per kilogram of O_2 captured can be calculated. Specific regeneration energy (Q_{thermal}) is reported as the sum of the energy required to heat the adsorbent to the desorption temperature, and the energy required to desorb bound gas species from the adsorbent,¹¹ according to the equation:

$$Q_{\text{thermal}} = \frac{c_p m_{\text{sorbent}} \Delta T + (\Delta h O_2 \Delta q O_2)}{m O_2}$$

Where,

c_p = specific heat capacity of adsorbent ($\text{Jg}^{-1}\text{K}^{-1}$)

m_{sorbent} = mass of adsorbent (g)

ΔT = Temperature difference between adsorption and desorption conditions (K)

Δh = heat of adsorption (kJmol^{-1})

Δq = working capacity, it can be defined as the difference between the O_2 loadings at adsorption and O_2 loadings at the end of desorption¹².

$m O_2$ = Mass of oxygen adsorbed at that pressure (g)

Applying this equation to 0.1320 g of **MFC4**, the MOF composite with **12.18** wt. % of Fe_3O_4 nanoparticles, the energy required to regenerate the amount of oxygen captured at 200 mbar, 400 bar, 800 mbar and 1000 mbar is calculated and the values are:

Pressure (mbar)	Δq (mmol/g)	Calculated Regeneration energy (MJ/kg)
200	0.93	2.89
400	1.98	1.67
800	3.5	1.20
1000	4.2	1.10

While this calculation does not include process considerations and cooling duty of air from ambient to 204 K, we expect this energy requirement to be less than half of that required for cryogenic distillation at 92 K. Using a suitable fraction of the above quoted energy costs for Cryogenic distillation, and without further improvements to the technology, the total estimated energy cost of the MISA process for capturing oxygen from air from lab scale experiments is broadly competitive to the mature process. However, with orders of magnitude increases in scale, we expect the efficiency using this first generation material to greatly improve. Further efficiencies may be achieved through operation at higher pressures, as is indicated by the trends in working capacity (Δq) and regeneration energy with pressure.

References:

1. Adhikari, A. K.; Lin, K.-S., Improving CO₂ adsorption capacities and CO₂/N₂ separation efficiencies of MOF-74(Ni, Co) by doping palladium-containing activated carbon. *Chem. Eng. J.* **2016**, 284, 1348-1360.
2. Grant Glover, T.; Peterson, G. W.; Schindler, B. J.; Britt, D.; Yaghi, O., MOF-74 building unit has a direct impact on toxic gas adsorption. *Chem. Eng. Sci.* **2011**, 66, (2), 163-170.
3. Hui, C.; Shen, C.; Yang, T.; Bao, L.; Tian, J.; Ding, H.; Li, C.; Gao, H. J., Large-Scale Fe₃O₄ Nanoparticles Soluble in Water Synthesized by a Facile Method. *J. Phys. Chem. C* **2008**, 112, (30), 11336-11339.
4. Howarth, A. J.; Peters, A. W.; Vermeulen, N. A.; Wang, T. C.; Hupp, J. T.; Farha, O. K., Best Practices for the Synthesis, Activation, and Characterization of Metal–Organic Frameworks. *Chem. Mater.* **2017**, 29, (1), 26-39.
5. Zhang, Y.; Zhai, Y., Magnetic induction heating of nano-sized ferrite particle. In *Adv. Ind. Micro. Heat. Mine. Organ. Mater.*, InTech: 2011.
6. Ebrahimi, M., On the temperature control in self-controlling hyperthermia therapy. *J. Magn. Mater.* **2016**, 416, 134-140.
7. Kolhatkar, A.; Jamison, A.; Litvinov, D.; Willson, R.; Lee, T., Tuning the Magnetic Properties of Nanoparticles. *Int J Mol Sci* **2013**, 14, (8), 15977.
8. Sun, S.; Liu, C.; Peng, R.; Fu, Z.; Lu, Y., Measuring room-temperature intrinsic multiferroic properties by excluding the secondary magnetic inclusion contribution. *Sci. China. Mater.* **2015**, 58, (10), 791-798.
9. Kekalo, K.; Baker, I.; Meyers, R.; Shyong, J., Magnetic Nanoparticles with High Specific Absorption Rate at Low Alternating Magnetic Field. *Nano LIFE* **2015**, 5, (2), 1550002.
10. Mornet, S.; Vasseur, S.; Grasset, F.; Duguet, E., Magnetic nanoparticle design for medical diagnosis and therapy. *J. Mater. Chem.* **2004**, 14, (14), 2161-2175.
11. Sadiq, M. M.; Li, H.; Hill, A. J.; Falcaro, P.; Hill, M. R.; Suzuki, K., Magnetic Induction Swing Adsorption: An Energy Efficient Route to Porous Adsorbent Regeneration. *Chem. Mater* **2016**, 28, (17), 6219-6226.
12. Zhang, W.; Liu, H.; Sun, Y.; Cakstins, J.; Sun, C.; Snape, C. E., Parametric study on the regeneration heat requirement of an amine-based solid adsorbent process for post-combustion carbon capture. *Appl. Ener.* **2016**, 168, 394-405.

Appendix A

Table A.1. Nitrogen Isotherms at 77K for Bare Co-MOF-74.

Relative Pressure (P/P₀)	Absolute Pressure (mbar)	Quantity Adsorbed (mmol/g)
0.000977955	0.987900146	15.63518543
0.001181066	1.192961455	15.79217896
0.001293304	1.30657671	15.86303329
0.001462071	1.476998322	15.96156393
0.001728164	1.745795452	16.09122058
0.001935408	1.95501444	16.17074877
0.002205617	2.227969249	16.26153386
0.002582891	2.608995741	16.3645193
0.002932798	2.962312002	16.44417384
0.003419659	3.454181964	16.53294422
0.003879597	3.918341695	16.60281744
0.004595425	4.641599847	16.68785136
0.005171082	5.222149162	16.74549783
0.005998176	6.057636676	16.81156283
0.006856942	6.924992102	16.8714284
0.007956555	8.034820318	16.92989503
0.009085723	9.175133096	16.98310165
0.010528328	10.63134811	17.03837356
0.012058516	12.17623993	17.08646032
0.013923869	14.05920319	17.13613916
0.015984224	16.13891749	17.1824707
0.018430861	18.60797363	17.22926146
0.021154039	21.35690897	17.2741013
0.024342284	24.57278091	17.31871904
0.027940033	28.20292551	17.36315135
0.032114358	32.41639122	17.40650763
0.036870824	37.21317803	17.44984728
0.042429632	42.82466395	17.49371741
0.048696949	49.14972204	17.53686519
0.052340033	52.8255884	17.55948821
0.056277273	56.7993531	17.58449728
0.064294486	64.88682464	17.62574382
0.069228224	69.86234841	17.65056055
0.074108534	74.77828642	17.67405347
0.084809554	85.57589846	17.7153447
0.097655219	98.5322029	17.75986769
0.105079101	106.0128008	17.78515678

0.112398835	113.3825577	17.80820879
0.128863579	129.9897876	17.85328557
0.138716537	139.9325248	17.87967744
0.148364777	149.6535701	17.90353336
0.170056792	171.5231247	17.94953887
0.183077238	184.6387687	17.97586368
0.195683392	197.3429067	18.00141986
0.224438002	226.3244981	18.0492475
0.258000037	260.1610991	18.09636894
0.296393734	298.8623524	18.14248386
0.340486039	343.3247503	18.19109603
0.391060921	394.2978651	18.23957948
0.449203175	452.9220045	18.2886503
0.516102535	520.3845711	18.33854894
0.535406783	539.7975298	18.36190778
0.5548932	559.4321908	18.37687576
0.593035455	597.8715841	18.40662045
0.615277523	620.213624	18.42988367
0.637371398	642.4794575	18.45469883
0.68149364	686.9875263	18.49146416
0.706851603	712.4997571	18.52312205
0.732390868	738.2696164	18.55071158
0.783162524	789.3604787	18.59135771
0.831387764	837.961555	18.6299541
0.841423388	848.0566744	18.6557475
0.899806611	906.8650841	18.70521874
0.849929467	856.617984	18.71036352
0.819270995	825.6315114	18.71587756
0.788400065	794.5341267	18.73066356
0.757763229	763.6557182	18.73220128
0.727123796	732.7426446	18.73196528
0.696300951	701.6660915	18.73116234
0.66555187	670.689343	18.72933325
0.634897402	639.7735027	18.72557049
0.604270054	608.8839867	18.72098463
0.573656177	577.9972374	18.70668824
0.562191162	566.3945919	18.70722335
0.51218173	515.9798623	18.68771001
0.500813189	504.5074958	18.68765524
0.450909157	454.2271953	18.65909259
0.43940015	442.6328906	18.65524793
0.389459142	392.3082008	18.62417243
0.37808564	380.8330676	18.62126744
0.327930568	330.3171907	18.58822894
0.316740731	319.0498856	18.5800901

0.286131306	288.192207	18.55418294
0.255525167	257.356723	18.52408131
0.224908381	226.5295594	18.48806356
0.194284941	195.680242	18.44961073
0.163598315	164.7616248	18.40201043
0.132851151	133.7973061	18.34082936
0.102146092	102.8675916	18.26363391
0.07159233	72.10000874	18.15798188
0.041028895	41.31995794	17.99340131
0.010298489	10.37224969	17.55516245

Table A.2. Nitrogen Isotherms at 77K of the magnetic composite MC1 with 0.08 wt. % nanoparticles.

Relative Pressure (P/Po)	Absolute Pressure (mbar)	Quantity Adsorbed (mmol/g)
0.000956185	0.956510305	16.46981747
0.001113003	1.11315436	16.6108737
0.001275239	1.275347073	16.74307236
0.001476239	1.476349877	16.88336984
0.001685418	1.685673124	16.99981308
0.001922385	1.922724404	17.1145731
0.002267413	2.267900768	17.24931301
0.002565026	2.565941512	17.33936453
0.002923195	2.924981893	17.43413795
0.003461134	3.462845703	17.5471541
0.003881016	3.882880634	17.62366971
0.004400342	4.402725291	17.69782647
0.005057895	5.061189766	17.77850719
0.005933393	5.935914582	17.86469621
0.006798113	6.800935604	17.9342647
0.007800622	7.804576444	18.0032922
0.009035579	9.041113426	18.07388984
0.010375361	10.38299862	18.13701961
0.01187873	11.88846497	18.19841992
0.013761662	13.77376263	18.26269034
0.015805068	15.81848122	18.32205626
0.018177387	18.19728395	18.38141125
0.020940001	20.96146665	18.43956359
0.024077537	24.10131536	18.49616647
0.027702235	27.72913065	18.55311128
0.031908674	31.93916849	18.60932563

0.036678956	36.71202131	18.66434787
0.042166539	42.20572159	18.72012359
0.048582358	48.62682587	18.77590129
0.052175039	52.22830665	18.80428317
0.056718046	56.78351577	18.83858104
0.064232806	64.30114879	18.8878685
0.069460669	69.54393377	18.91948068
0.074408642	74.50393555	18.94800862
0.084718313	84.83010493	19.00101258
0.097855656	97.96480558	19.05980803
0.105843619	105.9662348	19.09264727
0.11321324	113.3480045	19.12197632
0.1285698	128.7187431	19.17554688
0.139262957	139.4136465	19.20976424
0.14884292	149.0120415	19.23958484
0.169654106	169.8487523	19.29642678
0.183527694	183.7431105	19.33151562
0.196327116	196.5548244	19.3625586
0.223917371	224.2063247	19.42237245
0.257818403	258.1500132	19.48805298
0.296167328	296.5491063	19.55410947
0.340248165	340.6692674	19.62293424
0.390235185	390.7571805	19.69406099
0.448419575	449.046183	19.77111446
0.515215359	515.9395824	19.85437224
0.535071879	535.8433457	19.88076012
0.554451129	555.2467024	19.90634497
0.592348119	593.2021672	19.95687864
0.614843583	615.7522792	19.98869305
0.637048994	637.9807623	20.02139403
0.680257049	681.3399182	20.08893307
0.706363454	707.4859267	20.13583607
0.73182201	732.9859514	20.18510372
0.780904508	782.1562355	20.29761644
0.811353614	812.6384363	20.38285646
0.840344531	841.7441224	20.47791279
0.894961084	896.5771908	20.70386439
0.853325217	854.8815541	20.59629862
0.822144972	823.5759345	20.50888433
0.79101984	792.4185775	20.42973722
0.77768442	779.1535521	20.39705337
0.74731015	748.6533678	20.33016637
0.716665905	718.0546401	20.26381911
0.68575256	687.0623086	20.20309923
0.655087825	656.3417241	20.14863814

0.624218012	625.4449251	20.10058345
0.593603773	594.7630744	20.05817909
0.562833133	563.9495613	20.0180443
0.532000376	533.0888922	19.9810118
0.501487097	502.4902052	19.94452878
0.472033936	473.0102416	19.87639705
0.44044	441.4176582	19.78566522
0.408713158	409.5976765	19.7368662
0.379501527	380.3381131	19.6955396
0.348082344	348.8661253	19.6514153
0.317421376	318.1233055	19.6051305
0.286553161	287.2127137	19.55675289
0.256008632	256.5932561	19.50405593
0.22530763	225.8268379	19.44519029
0.194650083	195.0964886	19.38054803
0.16403303	164.4174147	19.30620162
0.133422737	133.7327973	19.21844945
0.102871927	103.1105628	19.1121947
0.072562875	72.73231163	18.97229867
0.042522251	42.62160138	18.76452505
0.009752085	9.774436468	18.16392171